Astronomy & Astrophysics manuscript no. vonEssenC
April 12, 2019

Indications for transit timing variations in the exo-Neptune HAT-P-26b

C. von Essen[1,2], S. Wedemeyer[3], M. S. Sosa[4,5], M. Hjorth[1], V. Parkash[8], J. Freudenthal[7], M. Mallonn[9], R. G. Miculán[4,5], L. Zibecchi[4,5], S. Cellone[4,6], A. F. Torres[4,5]

[1]Stellar Astrophysics Centre, Department of Physics and Astronomy, Aarhus University, Ny Munkegade 120, DK-8000 Aarhus C, Denmark
[2]Astronomical Observatory, Institute of Theoretical Physics and Astronomy, Vilnius University, Sauletekio av. 3, 10257, Vilnius, Lithuania
[3]Institute of Theoretical Astrophysics, University of Oslo, Postboks 1029 Blindern, N-0315 Oslo, Norway
[4]Facultad de Ciencias Astronómicas y Geofísicas, Universidad Nacional de La Plata, Paseo del Bosque, B1900FWA, La Plata, Argentina
[5]Instituto de Astrofísica de La Plata (CCT-La Plata, CONICET-UNLP), Paseo del Bosque, B1900FWA, La Plata, Argentina
[6]Consejo Nacional de Investigaciones Científicas y Técnicas, Godoy Cruz 2290, C1425FQB, Ciudad Autónoma de Buenos Aires, Argentina
[7]Institut für Astrophysik, Georg-August-Universität Göttingen, Friedrich-Hund-Platz 1, 37077 Göttingen, Germany
[8]Monash Centre for Astrophysics, School of Physics and Astronomy, Monash University, Victoria 3800, Australia
[9]Leibniz-Institut für Astrophysik Potsdam, An der Sternwarte 16, 14482, Potsdam, Germany
e-mail: cessen@phys.au.dk

Received XXXX; accepted XXXX

ABSTRACT

From its discovery, the low density transiting Neptune HAT-P-26b showed a 2.1σ detection drift in its spectroscopic data, while photometric data showed a weak curvature in the timing residuals that required further follow-up observations to be confirmed. To investigate this suspected variability, we observed 11 primary transits of HAT-P-26b between March, 2015 and July, 2018. For this, we used the 2.15 meter Jorge Sahade Telescope placed in San Juan, Argentina, and the 1.2 meter STELLA and the 2.5 meter Nordic Optical Telescope, both located in the Canary Islands, Spain. To add upon valuable information on the transmission spectrum of HAT-P-26b, we focused our observations in the *R*-band only. To contrast the observed timing variability with possible stellar activity, we carried out a photometric follow-up of the host star along three years. We carried out a global fit to the data and determined the individual mid-transit times focusing specifically on the light curves that showed complete transit coverage. Using bibliographic data corresponding to both ground and space-based facilities, plus our new characterized mid-transit times derived from parts-per-thousand precise photometry, we observed indications of transit timing variations in the system, with an amplitude of ~4 minutes and a periodicity of ~270 epochs. The photometric and spectroscopic follow-up observations of this system will be continued in order to rule out any aliasing effects caused by poor sampling and the long-term periodicity.

Key words. stars: planetary systems – stars: individual: HAT-P-26 – methods: observational

1. Introduction

From the first exoplanets ever detected around other stars than our Sun, the most successful exoplanet detection methods have been the radial velocity (RV, such as Butler et al. 2006) and the transit (Charbonneau et al. 2000, and onward) techniques. The main engine of this work, the *Transit Timing Variation* method (TTV), gained special relevance with the advent of the Kepler space telescope (Borucki et al. 2010; Koch et al. 2010). For this technique, once an exoplanet is detected via the transit method, the variations of the observed mid-transit times allow the subsequent detection and/or characterization of further transiting (Carter et al. 2012) and non-transiting (Barros et al. 2014) exoplanets. The technique is sensible to planets with masses as low as an Earth mass (Agol et al. 2005), which would be extremely challenging to detect or characterize by means of other techniques. The TTV method requires sufficiently long baseline, precise photometry, and good phase coverage. All these requirements are satisfied by Kepler data (see e.g., Mazeh et al. 2013, for a TTV characterization of hundreds of Kepler Objects of Interest, KOIs). As a consequence, surveys focused on TTVs from the ground have been mainly carried out photometrically following-up hot Jupiters with deep transits orbiting bright stars (e.g., Maciejewski et al. 2011; Fukui et al. 2011; von Essen et al. 2013). Nonetheless, none of them revealed unquestionable detection of TTVs. On the contrary, TTVs in the Kepler era revealed that multiple systems are not rare at all, and that most of the planets in these multiple systems are within the Super Earth/mini Neptune regime (see Holman et al. 2010; Lissauer et al. 2011; Cochran et al. 2011). Thus, from Kepler results we can re-focus our observing capabilities and boost our success rate from the ground by programming photometric follow-ups of more suitable transiting systems, including the Neptune planets instead of hot Jupiter ones.

Between 2015 and 2018 our group carried out a photometric follow-up of three Neptune-sized exoplanetary systems. The observations were mainly focused around primary transits. These

Send offprint requests to: cessen@phys.au.dk

systems presented either "hints" of multiplicity, or showed orbital and physical parameters similar to KOIs in multiple systems with large amplitude TTVs. Here we present our efforts in the detection of TTVs in HAT-P-26b, which is one of such aforementioned systems. HAT-P-26b, a low-density Neptune-mass planet transiting a K-type star, was discovered in 2011 by the HATNet consortia (Hartman et al. 2011). Once the spectral reconnaissance was carried out, additional high-resolution spectra were acquired to better characterize the RV variations and the stellar parameters. The spectroscopic analysis revealed a chromospherically quiet star, along with a Neptune-mass planet orbiting its host star each ∼4.23 days. A combined analysis between photometric and spectroscopic data provided better constraints on the planetary mass and radius. Further analysis of spectroscopic data revealed a 2.1σ detection drift in its RVs. Nonetheless, the data were not sufficient to characterize the system's multiplicity. Furthermore, Stevenson et al. (2016) observed a weak curvature in the timing residuals of HAT-P-26b, but yet again without proper confirmation due to insufficient data. Although the $\Delta F = 0.53\%$ transit depth makes the transit challenging to be observed using ground-based facilities, the observed RV drift and curvature in the timing residuals makes HAT-P-26b an interesting system for TTV studies. To confront the TTV detection with other possible sources of variability, we also carried out a photometric follow-up of the host star along three years.

Besides TTV analysis, several efforts were produced to characterize the chemical constituents of the atmosphere of HAT-P-26b. While Stevenson et al. (2016) found tentative evidence for water and a lack of potassium in transmission, Wakeford et al. (2017) measured HAT-P-26b's atmospheric heavy element content and characterized its atmosphere as primordial. The observations presented here were focused solely in the *R*-band. Thus, besides the TTV discovery and characterization, in this work we also provide an accurate wavelength-dependent planet-to-star radii ratio around the Johnson-Cousins *R* band, 635 ± 100 nm, in order to contribute with its exo-atmospheric characterization.

In this work, Section 2 details our observations and specifies the data reduction techniques. Section 3 shows the steps involved in the transit analysis and the derived model parameters. Section 4 shows our results on TTVs, and we finish with a brief discussion and our conclusions in Section 5.

2. Observations and data reduction

2.1. Observing sites and specifications of the collected data for transit photometry

Between March, 2015 and July, 2018 we observed HAT-P-26 (R = 11.56, V = 11.76, Høg et al. 2000) during ten primary transits. Our observations were performed using the 2.15 meter Jorge Sahade Telescope located at the Complejo Astronómico El Leoncito[1] (CASLEO) in San Juan, Argentina, the 2.5 meter Nordic Optical Telescope[2] (NOT) located in La Palma, Spain, and the 1.2 meter STELLA, located in Tenerife, Spain. The most relevant parameters of our observations are summarized in Table 3.1. All the observations were carried out using a Johnson-Cousins *R* filter, to minimize the impact of our Earth's atmosphere in the overall signal-to-noise ratio of our measurements circumventing telluric lines and the strong absorption of stellar light caused by Rayleigh scattering. Also, several transits allowed us to accurately characterize the planetary size within that wavelength range. To increase the photometric precision of our data all telescopes were slightly defocused (Kjeldsen & Frandsen 1992; Southworth et al. 2009). In consequence, values of seeing taken from science frames are not representative of the quality of the sky at both sites. Table 3.1 shows then only intra night variability of the seeing. Exposure times were typically set between 10 and 60 seconds, and the photometric precision ranged between 1.1 and 3.7 parts-per-thousand (ppt), in all cases below the transit depth (∼5.3 ppt). Seven light curves show complete transit coverage. The rest show partial transit coverage mainly due to poor weather conditions.

During each observing night we obtained a set of 15 bias and between 10 to 15 twilight sky flats. Due to low exposure times and optimum cooling of charge-coupled devices, we did not take dark frames. In the case of CASLEO data we observed using a focal reducer. This produces an unvignetted field of view of 9 arcmin of diameter, allowing the simultaneous observation of HAT-P-26 along with two reference stars of similar brightness, namely TYC 320-426-1 (V = 11.08, Høg et al. 2000) and TYC 320-1376-1 (V = 12.5, Høg et al. 2000), also observed by STELLA. On the contrary, the size of the field of view of the NOT is about 7 arcmin^2. Therefore, we only observed TYC 320-426-1 and fainter reference stars simultaneously to HAT-P-26.

2.2. Transit data reduction and preparation

For details on the data reduction, we refer the reader to the description of DIP^{2}OL (von Essen et al. 2018). In brief, all the science frames were bias and flat field calibrated using the IRAF task *ccdproc*. Owed to the large availability of calibration frames, we corrected the science frames of a given observing night with the calibrations taken during that particular night only. To produce photometric light curves we used the IRAF task *apphot*. We measured fluxes inside apertures centered on the target and all available reference stars within the field of view of the telescopes. Their sizes were set as a fraction of the full-width at half-maximum (FWHM) computed and averaged per night. In particular, the apertures were set between 0.7 and 5 times the FWHM, divided into 10 equally spaced steps. For each one of the apertures we chose three different sky rings, being their widths 1, 2, and 3 times the FWHM. The inner radii of the sky ring was fixed to 5 times the FWHM.

Next, we produced differential light curves for the target and each combination of reference stars by dividing the flux of the target by the average of a given combination of fluxes from the reference stars. For each one of the light curves we computed the standard deviation of the residuals, that were obtained dividing the differential light curve by a high-degree, time-dependent polynomial that was fitted to the whole data, including in-transit points, minimizing the sum of the squares of the residuals. In particular, the degree of the polynomial was chosen to account for the shallow transit depth and most of the systematic noise. After visually inspecting all the light curves, it was chosen to be a septic degree and was fixed along all the nights. The final combination of reference stars and aperture was chosen by minimizing the standard deviation of the residual light curves. This process was performed per transit, individually. With the time set in Julian dates and the differential fluxes defined, we finally changed the magnitude of the error bars provided by the *apphot*

[1] Visiting Astronomer, Complejo Astronómico El Leoncito operated under agreement between the Consejo Nacional de Investigaciones Científicas y Técnicas de la República Argentina and the National Universities of La Plata, Córdoba and San Juan; www.casleo.gov.ar

[2] not.iac.es

Table 1: Relevant parameters of our observations. From left to right: the date corresponding to the beginning of the local night in yyyy.mm.dd, the telescope performing the observations, the standard deviation of the residual light curves in parts-per-thousand (ppt), σ_{res}, the number of data points per light curve, N, the average cadence in seconds, CAD, the total observing time, T_{tot}, in hours, the airmass range, $\chi_{max,min}$, showing maximum and minimum values, the β factor, to quantify correlated noise, the maximum variability in pixel position, Δpix, considering both x and y shifts, and the maximum variability in seeing, Δs, in pixels. Both values are rounded up. Last column shows the transit coverage, TC; a description of the transit coding is detailed in the footnote of this table.

Date yyyy.mm.dd	Telescope	σ_{res} (ppt)	N	CAD (sec)	T_{tot} (hours)	$\chi_{max,min}$	β	Δpix ($max_{x,y}$)	Δs (pix)	TC
2015.03.30	CASLEO	1.8	597	25	4.31	1.53,1.23	2.33	40	3	OIBEO
2015.04.12	NOT	0.8	843	18	4.24	2.33,1.10	2.00	4	3	OIBEO
2015.04.16	CASLEO	1.6	307	74	6.28	1.94,1.23	2.15	50	6	OIBEO
2015.05.20	NOT	1.8	482	19	2.67	1.82,1.13	1.62	3	2	OIBE-
2015.06.06	NOT	3.1	943	15	3.91	2.95,1.12	1.19	4	4	OIBEO
2015.06.23	NOT	2.0	977	14	3.81	2.33,1.10	1.47	2	2	OIBEO
2016.05.14	CASLEO	1.9	372	36	3.77	2.13,1.23	1.51	120	8	-IBEO
2017.05.13	CASLEO	3.3	289	63	5.12	2.03,1.23	2.59	52	3	OIBEO
2017.05.30	CASLEO	1.8	742	22	4.58	1.94,1.23	2.84	35	3	OIBEO
2017.06.16	CASLEO	1.9	174	52	2.53	1.31,1.23	1.42	30	3	OIB- -
2018.07.01	STELLA	1.2	141	112	4.42	1.98,1.09	1.75	350	6	–BEO

Notes. The letter code to specify the transit coverage during each observation is the following: O: out of transit, before ingress. I: ingress. B: flat bottom. E: egress. O: out of transit, after egress.

task so that their averaged magnitude was coincident with the standard deviation of the data. Besides time, flux and errors, we also computed (x,y) centroid positions, integrated flat counts in the selected aperture around those (x,y) positions, the seeing, the airmass, and the background counts inside the selected sky ring, all of them as a function of time and for all the stars involved in the selected differential light curve.

2.3. Data reduction of the long-term monitoring of HAT-P-26

Stellar activity, and particularly stellar spots rotating with the star, can mimic transit timing variations (see Section 4.2). As part of the VAriability MOnitoring of exoplanet host Stars (VAMOS) project, we carried out a photometric follow-up of the host star, HAT-P-26, along three years. For this end we observed with the wide-field imager WIFSIP mounted at the 1.2 meter twin-telescope STELLA, located in the Canary Islands, Spain (Strassmeier et al. 2004; Weber et al. 2012). Table 2 shows the main characteristics of the observations. The data were reduced using standard routines of ESO-MIDAS. On average, around five stars were used to construct the differential light curve. For details on the data reduction steps, we refer the reader to Mallonn et al. (2015) and Mallonn & Strassmeier (2016).

Table 2: Main characteristics of the observations performed with STELLA. From left to right: time range, Δt in dd.mm.yyyy, photometric bands, PB, exposure time in seconds, t_{exp}, minimum and maximum exposures taken per filter and per night $N_{min/max}$, total number of nightly averaged data points, N_{av}, and standard deviation of the light curves per observing season in ppt, σ_{phot}.

Δt	PB	t_{exp}	$N_{min/max}$	N_{av}	σ_{phot}
21.03.2012 - 16.08.2012	V	30	3/36	51	2.1
21.03.2012 - 16.08.2012	I	30	3/36	45	2.1
09.04.2016 - 29.07.2016	B	40	3/4	48	2.3
09.04.2016 - 29.07.2016	V	30	3/4	48	2.2
25.02.2017 - 05.08.2017	B	40	3/4	67	2.3
25.02.2017 - 05.08.2017	V	30	3/4	62	2.2

Notes. dd.mm.yyyy corresponds to the day (dd), month (mm) and year (yyyy) in which the observations were performed.

3. Model parameters and transit analysis

3.1. Choice of detrending model and correlated noise treatment

To clean the data from systematics we constructed an initial detrending model, DM, with their terms represented by a linear combination of seeing, S, airmass, χ, (x,y) centroid positions of all the stars involved in the creation of the differential light curves, and their respective integrated flat counts and background counts around these positions, henceforth, the detrending components:

$$DM(t) = a_0 + a_1 \cdot S + a_2 \cdot \chi + \sum_{1}^{N+1} c_i \cdot BG_i + d_i \cdot FC_i + e_i \cdot X_i + f_i \cdot Y_i \quad (1)$$

Here, N is the total number of reference stars. N+1 includes the components of the target star, too. X_i and Y_i correspond to the (x,y) centroid positions, FC_i to the integrated flat counts, and BG_i to the background counts. The coefficients of the detrending model are a_0, a_1, a_2, and d_i, e_i and f_i, with i = 1, N+1. **Besides this linear combination, we also considered time-dependent polynomials with degrees ranging from one to three. The detrending strategy is fully described in von Essen et al. (2018).** In an iterative process we defined a joint model conformed by the transit model (see Section 3.2 for details) times the detrending model. During each iteration, **where we evaluated the different time-dependent polynomials and the different combinations of detrending components,** we computed reduced χ^2, the Bayesian Information Criterion (see e.g., von Essen et al. 2017,

for details on its use) and the weighted standard deviation between the transit photometry and the combined model. In all these statistical indicators, the number of fitting parameters are taken into consideration. Thus, we took care that the data were not being over-fitted by an unnecessary large detrending model. After averaging the three statistical indicators, we chose as final detrending model (and thus, the final number of detrending components **or the final degree for the time-dependent polynomial**) the one that minimized this averaged statistic. Usually the airmass, the (x,y) centroid positions and the integrated flat counts of all the stars involved in the construction of the differential light curves were part of the chosen detrending model. **For the Nordic Optical Telescope data, that counts with an excellent tracking system, a second order, time-dependent polynomial was usually sufficient to account for instrumental systematics.** Once the detrending model was defined, we treated correlated noise as specified in von Essen et al. (2013). In brief, following Carter & Winn (2009) we produced residual light curves, subtracting the primary transit model from the data (Mandel & Agol 2002). As orbital parameters we used bibliographic values, listed in this work in the first column of Table 3. We then divided each light curve into M bins of equal duration, each bin holding an averaged number of N data points. An averaged N accounts for non-equally spaced data points. If the data is free of correlated noise, then the noise within the the residual light curves should follow the expectation of independent random numbers $\hat{\sigma_N}$,

$$\hat{\sigma_N} = \sigma_1 N^{-1/2}[M/(M-1)]^{1/2} . \quad (2)$$

Here, σ_1 is the sample variance of the unbinned data and σ_N is the sample variance (or RMS) of the binned data:

$$\sigma_N = \sqrt{\frac{1}{M}\sum_{i=1}^{M}(<\hat{\mu_i}> - \hat{\mu_i})^2} , \quad (3)$$

where the mean value of the residuals per bin is given by $\hat{\mu_i}$, and $<\hat{\mu_i}>$ is the mean value of the means. When correlated noise can not be neglected, each σ_N differs by some factor β_N from their expectation $\hat{\sigma_N}$. We computed β averaging the β_N's obtained over time bins close to the duration of HAT-P-26b's transit ingress (or, equivalently, egress), which is estimated to be ~15 minutes. To estimate β, we used as time-bin 0.8, 0.9, 1, 1.1, and 1.2 times the duration of ingress. Finally, we enlarged the magnitude of the error bars by β (Pont et al. 2006). On average, CASLEO data presented slightly more correlated noise (β ~2.1) compared to the NOT (β ~1.5). This is explained by guiding of the stars (see column eight of Table for a measurement of the amplitude of variability of the centroid position of the stars). While the NOT has a stable guiding system, CASLEO lacks of guiding and the telescope slightly tracks in the East-West direction, affecting more the quality of the photometry.

3.2. Transit fitting

With the ten light curves fully constructed, we converted the time stamps from Julian dates to Barycentric Julian dates, BJD_{TDB}, using the web tool provided by Eastman et al. (2010). The first step was to determine the expectation values of the model parameters of HAT-P-26b. For this end, we carried out a Markov-chain Monte Carlo (MCMC) global fit, using the `PyAstronomy`[3] packages (Patil et al. 2010; Jones et al. 2001). As transit model we used the one provided by Mandel & Agol (2002), along with a quadratic limb-darkening law. In particular, for the Mandel & Agol (2002) transit model the fitting parameters are the inclination in degrees, i, the semi-major axis in stellar radius, a/R_S, the orbital period in days, Per, the planet-to-star radii ratio, R_P/R_S, the mid-transit time in BJD_{TDB}, T_0, and the linear and quadratic limb darkening coefficients, u_1 and u_2.

The quadratic limb-darkening coefficients were taken from Claret (2000), for the Johnson-Cousins R filter and stellar parameters closely matching the ones of HAT-P-26 (T_{eff} = 5079 ± 88 K, [Fe/H] = -0.04 ± 0.08, and log(g) = 4.56 ± 0.06, Hartman et al. 2011). Thus, the values for the limb-darkening coefficients used in this work correspond to the stellar parameters T_{eff} = 5000 K, [Fe/H] = 0 and log(g) = 4.5, and are listed in Table 3. In this work, quadratic limb darkening coefficients are considered as fixed values. Nonetheless, to test if the adopted values for the limb darkening coefficients have an impact on the measured mid-transit times, we considered the linear and quadratic limb darkening values as fitting parameters as well. After carrying out a global fit including them in the fitting process, our posterior distributions for the parameters revealed values inconsistent with the spectral classification of the host star. Although our data present a photometric precision in the part-per-thousand level, the transit light curves are not precise enough to realistically fit for the limb darkening coefficients. Nonetheless, mid-transit times computed fitting for the limb darkening coefficients do not show a significant offset with respect to the ones computed fixing them, but slightly larger error bars.

To fit the data with our combined model, we began our analysis considering the transit parameters listed in Hartman et al. (2011), Stevenson et al. (2016) and Wakeford et al. (2017) as starting values. The adopted values are shown in the second column of Table 3. We chose uniform priors for the orbital period, and Gaussian priors for the semi-major axis, the inclination, and the planet-to-star radii ratio. To be conservative and avoid misleading the convergence of the fitting algorithm, as standard deviation for the Gaussian priors we chose three times the magnitude of the errors determined by the previously mentioned authors. The mid-transit time determined by Stevenson et al. (2016) has already five decimals of precision, which translates into an accuracy of ~2 seconds. Since this precision is significantly below our data cadence, throughout this work the reference mid-transit time is consider as fixed.

Once the priors were set, we iterated the fitting process 1.5×10^5 times. At each MCMC step not only the transit parameters are changed, but also the detrending coefficients are computed with the previously mentioned inversion techniques. Both transit parameters and detrending coefficients are saved at each MCMC step. When the total number of iterations were reached, we burned the initial 50 000 samples. From the mean values and standard deviations of the samples we computed the expectation values of the model parameters and their corresponding errors. The same process was done to determine the best-fit detrending coefficients. Throughout this work we provide the errors of the transit parameters at 1-σ level. As a consistency check we analyzed the posterior distributions to ensure convergence of the chains. To this end, we divided the chains in three equally large fractions, we computed the model parameters for each one of the sub-chains, and we checked that they were consistent within

[3] http://www.hs.uni-hamburg.de/DE/Ins/Per/Czesla/PyA/PyA/index.html

1-σ errors. Our best-fit values are listed in the third column of Table 3. To avoid visual contamination, not all the values for the transit parameters derived by other authors are displayed on Table 3. Nonetheless, the transit parameters presented in this work are in good agreement with all the bibliographic values. In particular, the value for the planet-to-star radii ratio follows the trend observed by Wakeford et al. (2017), and not the value reported by Hartman et al. (2011). Figure 1 shows one transit light curve and both model components isolated.

Table 3: Bibliographic and derived transit parameters of HAT-P-26b. H11 corresponds to Hartman et al. (2011), and S16 to Stevenson et al. (2016).

Parameter	Bibliographic values	This work
Per (days)	$4.2345023 \pm 7\times10^{-7}$ (S16)	$4.23450236 \pm 3\times10^{-8}$
a/R_S	11.8 ± 0.6 (S16)	12.05 ± 0.13
i (°)	87.3 ± 0.4 (S16)	87.31 ± 0.09
R_P/R_S	0.0737 ± 0.0012 (H11)	0.07010 ± 0.00016
T_0*	$5304.65218 \pm 2.5\times10^{-5}$ (S16)	Adopted from S16
u_1	-	0.5140 (fixed)
u_2	-	0.2180 (fixed)

Notes. T_0* corresponds to BJD_{TDB} - 2450000.

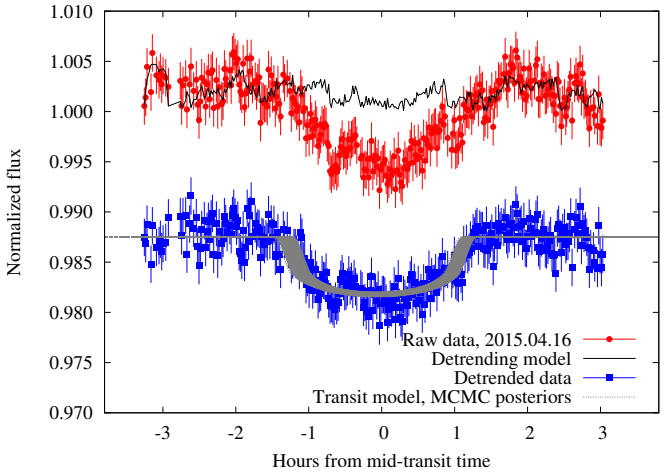

Fig. 1: Detrending process. The figure shows the evolution of the transit photometry during the fitting procedure. Raw data are plotted in red circles. The detrending model is plotted in black continuous line. Artificially shifted, the detrended data are plotted in blue squares, along with primary transit models which transit parameters are determined by the posterior distributions of the MCMC chains.

After producing a global fit to the complete data set (see Section 3.2), to characterize possible transit timing variations in the system we proceeded to fit the transits individually. Figure 2 shows the eleven transits, seven of them correspond to the JS telescope (red circles), one to STELLA (blue circles) and the remaining four to the NOT (green squares). To provide TTVs as realistic as possible, for this analysis **bf we fitted each individual transit. However, for a better assessment of the TTVs, complete and incomplete transits are clearly differentiated.**

To compute the mid-transit times of the individual light curves, rather than considering our best-fit model parameters as fixed, we used our global best-fit values and errors for the mean and standard deviation respectively for the Gaussian priors. For each individual mid-transit time we chose uniform priors. Since the determination of the individual mid-transit times requires the analysis of individual light curves, the orbital period was considered as fixed to the value derived from the global fit. This will properly propagate the uncertainties of all the transit parameters into the determination of the mid-transit times and, thus, will provide more realistic uncertainties. Equivalently to the global fit, we iterated and burned the same number of chains per light curve, and we computed the individual mid-transit times in the same fashion as specified in Section 3.2. For each light curve we also computed the transit parameters and we checked that they were consistent with the global ones, always at 1σ level. The first section of Table 4 shows the individual mid-transit times from the bibliography and their respective uncertainties, while the second section of the same table shows the mid-transit times and the uncertainties derived in this work.

Table 4: From left to right: calender date, epoch, mid-transit time in BJD_{TDB} - 2450000 along with 1σ uncertainties, and derived O-C values in minutes without uncertainties, to facilitate the comparison with Figure 3. The first section of the table shows bibliographic values taken from Hartman et al. (2011) (H11), Stevenson et al. (2016) (S16), and Wakeford et al. (2017) (W17). The second section are the values derived in this work. **The dates with an * correspond to mid-transit times derived from complete transits.**

Date yyyy.mm.dd	Epoch	Mid-transit time BJD_{TDB} -2450000	Uncertainty (days)	O-C (minutes)
Bibliographic values				
2009.01.28 (H11)	-105	4860.02786	0.00147	-3.3
2010.04.18 (S16*)	0	5304.65218	0.000025	-1.4
2010.05.25 (H11)	9	5342.76262	0.00041	-1.2
2013.04.23 (S16)	260	6405.6237	0.0009	1.3
2013.09.09 (S16)	293	6545.3622	0.0003	1.2
2015.04.16 (S16)	431	7129.72248	0.00017	-0.3
2016.01.25 (W17)	498	7413.432836	0.000172	-2.2
2016.03.12 (W17)	509	7460.013266	0.000016	-0.9
2016.05.02 (W17)	521	7510.827100	0.000016	-1.2
2016.08.16 (W17)	546	7616.690103	0.000011	-0.5
Our work				
2015.03.30*	427	7112.78503	0.00058	0.5
2015.04.12*	430	7125.48930	0.00063	1.6
2015.04.16*	431	7129.72283	0.00063	0.2
2015.05.20	439	7163.59738	0.00040	-1.9
2015.06.06*	443	7180.53670	0.00057	-0.03
2015.06.23*	447	7197.47376	0.00046	-1.4
2016.05.14	524	7523.53041	0.00072	-1.5
2017.05.13*	610	7887.69984	0.00089	1.7
2017.05.30*	614	7904.63796	0.00066	1.9
2017.06.16	618	7921.57698	0.00078	3.4
2018.07.01	690	8226.45772	0.00093	-1.6

Notes. The two transit times from H11 are not individually measured transit times, but rather two reference times which are used in place of the period and reference epoch when simultaneously fitting all of the data, and assuming a constant linear ephemeris. Since both epochs differ, this will produce a spurious offset in the O-C diagram (see epoch zero in Figure 3) unrelated to TTVs.

4. Analysis and results

4.1. Transit timing variations

We computed the TTVs in HAT-P-26b's system by subtracting to the observed mid-transit times the ones obtained from a con-

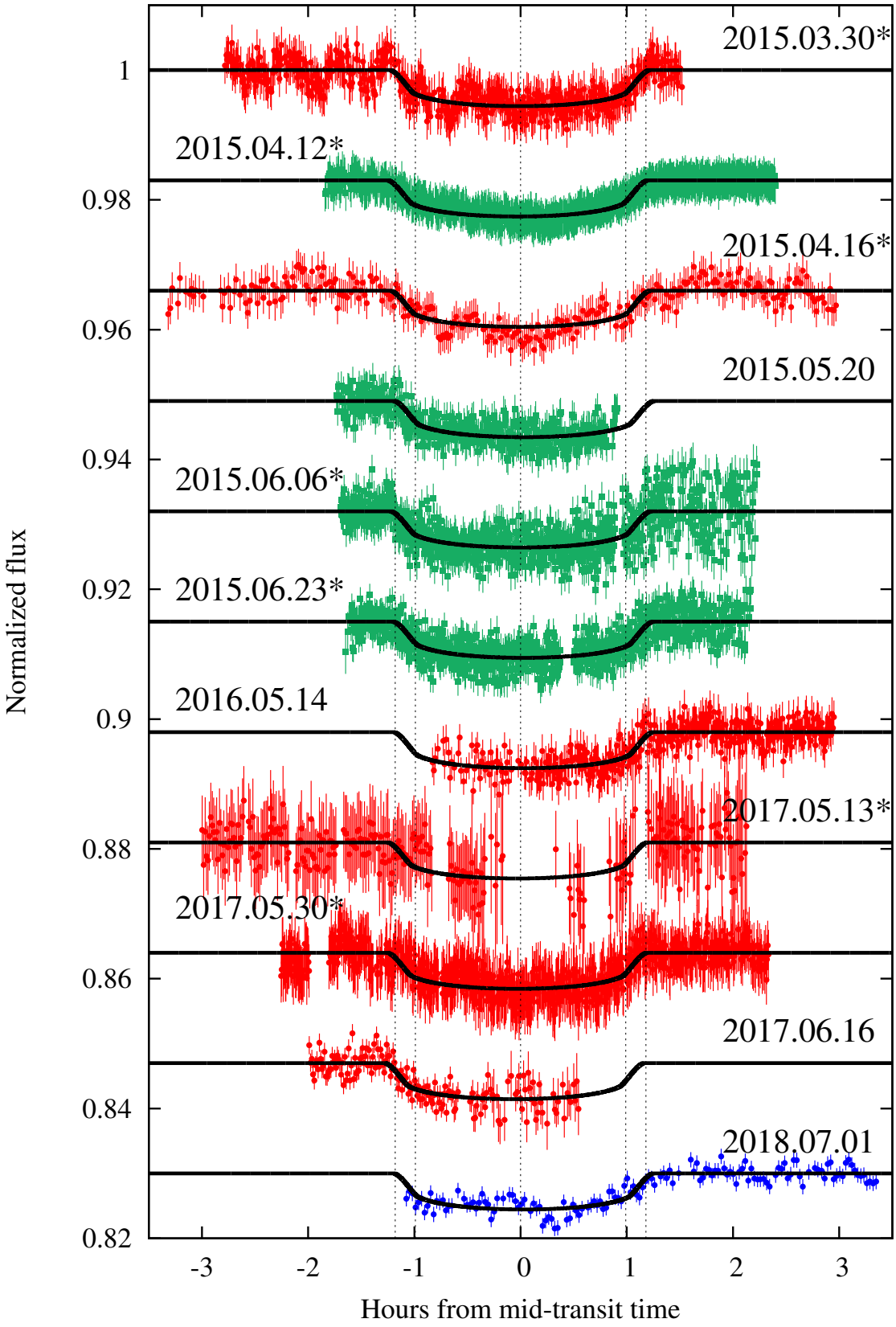

Fig. 2: The eleven transit light curves collected in this work. The transits observed with the Argentinian 2.15 meter telescope, CASLEO, are plotted in red circles. The ones taken with the Scandinavian 2.5 meter, NOT, are shown in green squares. The transit observed with STELLA is shown in blue circles. Calender dates are displayed, and asterisk, *, indicate the transits that are complete. Vertical dashed lines indicate the four contact times to guide the readers eyes. Transits have been folded using **our best-fit orbital period. In consequence, TTVs can be appreciated by comparing ingress or egress to the vertical dashed lines**.

stant (best-fit) orbital period. The derived values can be found on Figure 3 and the lower part of Table 4. Note that in the figure the zeroth epoch does not lie over the abscissas axis. This is due to the improvement of its value between Hartman et al. (2011) and Wakeford et al. (2017).

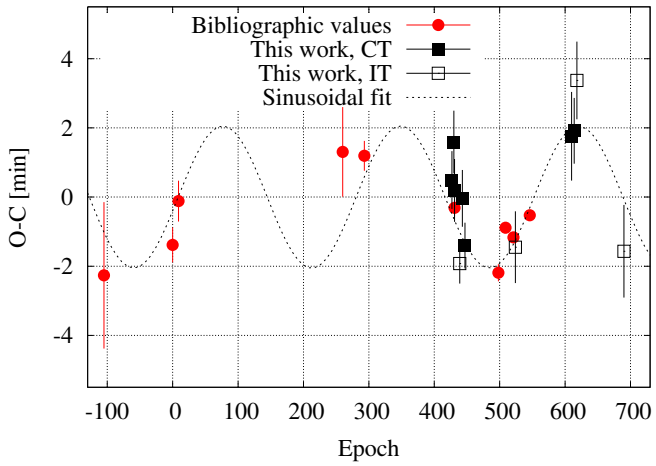

Fig. 3: Observed minus calculated (O-C) mid-transit times for HAT-P-26b in minutes. Red circular points show the values obtained from Hartman et al. (2011), Stevenson et al. (2016), and Wakeford et al. (2017). Black **filled squares correspond to the values derived in this work considering complete transits (CT), while empty squared are those derived from incomplete transits (IT)**. The O-C diagram was computed using the best-fit orbital period derived in this work, specified in Table 3. The dashed black line corresponds to our best-fit sinusoidal variability.

In the absence of any timing variations we expect no significant deviations of the derived O-C values from zero. To test the null hypothesis of O-C = 0, we used a χ^2_{red} test. For 20 degrees of freedom the value raises up to $\chi^2_{red} = 177$, with a p-value, P<1×10^{-5}. For this, the significance level is chosen to be 1%. This simple statistical analysis, χ^2_{red}, and its corresponding p-value indicate that the mid-transit times of HAT-P-26b are inconsistent with a constant period. A visual inspection of HAT-P-26b's O-C diagram suggests that the TTVs are strongly dependent on the last **three** data points. To test these assumptions we excluded the three last epochs and re-computed our statistics. A χ^2_{red} **= 102**, **P<1×10^{-5}**.

For completeness, assuming TTVs with a sinusoidal variability we fitted to our timing residuals a simple sinusoidal function with the following expression:

$$\mathrm{TTVs}(E) = A_{\mathrm{TTVs}} \sin[2\pi(E/Per_{\mathrm{TTVs}} - \phi_{\mathrm{TTVs}})]\,, \qquad (4)$$

where E corresponds to the epoch, A_{TTVs} corresponds to the semi-amplitude of the timing residuals, Per_{TTVs} to the periodicity, and ϕ_{TTVs} to the phase. From our analysis, we obtain A_{TTVs} ~2.1 minutes, while the best-fit periodicity would correspond to around 270 epochs. This is equivalent to almost 1100 days. Comparing the semi-amplitude with the average error bars for the timings we find A_{TTVs} ~3×ϵ, being ϵ the averaged value of the timing errors. Our best-fit sinusoidal function is plotted in Figure 3 with a black dashed line. Mainly due to possible aliasing effects, and due to the complications that single-transiting planets with TTVs convey, we believe any analysis on the TTVs reported in this work are subject to strong speculations. More spectroscopic and photometric data are required to characterize the body causing these TTVs.

4.2. TTVs induced by stellar activity

Due to the high photometric quality provided by space-based observations such as CoRoT (Auvergne et al. 2009) and Kepler, stellar magnetic activity and its impact on transit light curves have been studied in great detail. Dark spots and bright feculae on the stellar photosphere move as the star rotates, producing a time-dependent variation of the stellar flux. The photometric precision we can achieve nowadays is so high, that the small imprints of occulted spots on transit data have been used to characterize stellar surface brightness profiles and spot migration and evolution (see e.g., Carter et al. 2011; Sanchis-Ojeda et al. 2011; Sanchis-Ojeda & Winn 2011; Huber et al. 2010). When transit fitting is performed, an incorrect treatment of these "bumps" can have a significant impact on the computation of planetary and stellar parameters (see e.g., Czesla et al. 2009; Lanza 2011).

Occulted and unocculted spots can asymmetrically modify the shape of the transit light curves, and thus affect the true locations of the mid-transit times. Actually, the deformations that stellar activity produces on primary transits have been studied in detail and pinpointed in some cases as a misleading identification of TTVs (see e.g., Rabus et al. 2009). For example, Maciejewski et al. (2011) found TTVs in the WASP-10 system with an amplitude of few minutes. They attributed the variability to the gravitational interaction between the transiting planet and a second body of a tenth of a Jupiter mass close to a 5:3 mean motion resonance. Although Barros et al. (2013) did not find a linear ephemeris as a statistically good fit to the mid-transit times of WASP-10b, they showed that the observed variability could be produced by, for example, spot occultation features.

To quantify stellar activity in our system and support (or overrule) our TTV detection, we carried out a photometric follow-up of HAT-P-26 along three years (see e.g., Mallonn et al. 2015; Mallonn & Strassmeier 2016, Figure 4 and our Table 2). The data, taken in the Johnson-Cousins B, V, and I filters, show a maximum scatter of 2.3 ppt. To search for any significant periodicity contained in the data we computed Lomb-Scargle periodograms (Lomb 1976; Scargle 1982; Zechmeister & Kürster 2009), finding featureless periodograms within each observing season and within the whole observing run. As a consequence, the photometric follow-up of the host star seems to show no evidence of spot modulation. Nonetheless, the characterization presented in this work is as good as the data are. In other words, if spot induced modulation should exist, it would be well contained within the ~2 ppm limit.

Hartman et al. (2011) characterized the chromospheric activity of the star derived from the flux in the cores of the Ca II H and K lines, the so-called S index, $S_{HK} = 0.182 \pm 0.004$. Comparing this value to the relation between the S index and the stellar brightness variation found by Karoff et al. (2016) (their Figure 5), observational evidence should place the photometric variability of HAT-P-26 to be around 1 ppt. Assuming that spot modulation around and below this limit actually exists, and that it might have an impact on the TTVs, Ioannidis et al. (2016) found that the maximum amplitude of TTVs generated by spot crossing events strongly depends, among others, by the transit duration. In the case of HAT-P-26b (~143 minutes), TTVs caused by spots should have a maximum amplitude of ~1 minute. This is significantly below the TTV amplitude detected in this work.

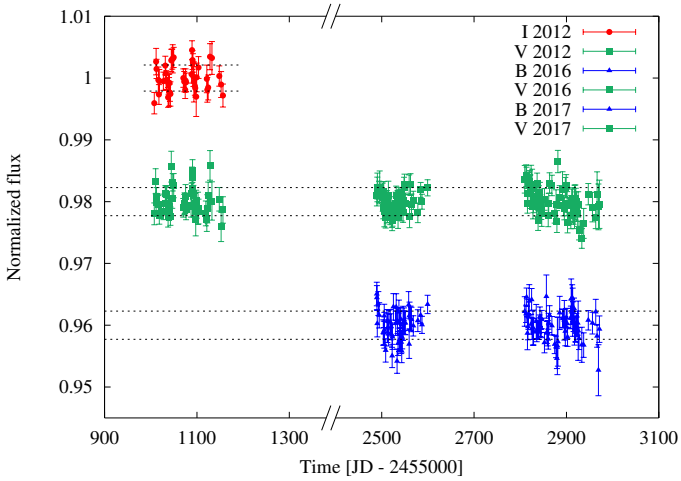

Fig. 4: Photometric follow-up of HAT-P-26 using the STELLA photometer. Red circles correspond to the *I* band, green squares to the *V* band, and blue triangles to the *B* band. The fluxes have been artificially shifted, and the time axis has been compressed for a better visualization. Dashed black lines show the averaged standard deviation.

Therefore, the data presented here seem to support the scenario of TTVs caused by gravitational interactions instead of modulated by the activity of the star, if any.

4.3. TTVs caused by systematic effects

Besides stellar activity, TTVs can be caused by systematic effects not properly accounted for. This has a special relevance when low-amplitude TTVs are being reviewed. A manifestation of this effect is the derivation of underestimated error bars for the mid-transit times. While in this work we have taken special attention to the computation of uncertainties, we can only trust that the values reported by other authors have had a similar treatment. Nonetheless, as a consistency check we enlarged the error bars of all the observed mid-transit times by a factor and re-computed χ^2_{red} for each one of the artificially enlarged O-C diagrams. A factor of 13 was required for χ^2_{red} to be consistent with 1, equivalently, with no TTVs. This marginally large value seems to support our TTV detection.

5. Discussion and conclusions

Since its discovery, some indications of variability in both spectroscopic and photometric data pinpointed HAT-P-26b as an interesting target for additional photometric follow-up. For the last three years our group has been collecting primary transit data of part-per-thousand photometric precision, necessary to detect the shallow transits that the planet produces while crossing its host star each ~4.23 days. In this work we have reduced all the new data in an homogeneous way, we have updated and improved the transit parameters and ephemeris, and we have detected a significant variability in the timing residuals. Furthermore, we have followed the host star along several years to characterize its activity and, if observed, its impact in the mid-transit times. However, light curves taken in three different bands along three years revealed no spot modulation within the precision limit of the data, devaluing the scenario of spot-induced TTVs. Due to the complexity of the analysis of single-transiting systems presenting TTVs, it is hard to drop any conclusions on the characteristics of the perturbing body. Nonetheless, we understand these results as relevant to motivate future photometric and spectroscopic follow-up campaigns, that will contribute to disclose the origin of the observed variability.

Acknowledgements. Visiting Astronomer, Complejo Astronómico El Leoncito operated under agreement between the Consejo Nacional de Investigaciones Científicas y Técnicas de la República Argentina and the National Universities of La Plata, Córdoba and San Juan. CvE acknowledges funding for the Stellar Astrophysics Centre, provided by The Danish National Research Foundation (Grant DNRF106), and support from the European Social Fund via the Lithuanian Science Council grant No. 09.3.3-LMT-K-712-01-0103. Based on observations made with the Nordic Optical Telescope, operated by the Nordic Optical Telescope Scientific Association at the Observatorio del Roque de los Muchachos, La Palma, Spain, of the Instituto de Astrofisica de Canarias. We acknowledge support from the Research Council of Norway's grant 188910 to finance service observing at the NOT. SW acknowledges support for International Team 265 ("Magnetic Activity of M-type Dwarf Stars and the Influence on Habitable Extra-solar Planets") funded by the International Space Science Institute (ISSI) in Bern, Switzerland. VP wishes to acknowledge the funding that was provided in part by a J. William Fulbright Grant and the sponsorship of Georg-August-Universitat in Gottingen, Germany. We thank the referee for the comments that contributed to improve this work. This work made use of PyAstronomy[4].

References

Agol, E., Steffen, J., Sari, R., & Clarkson, W. 2005, MNRAS, 359, 567
Auvergne, M., Bodin, P., Boisnard, L., et al. 2009, A&A, 506, 411
Barros, S. C. C., Boué, G., Gibson, N. P., et al. 2013, MNRAS, 430, 3032
Barros, S. C. C., Díaz, R. F., Santerne, A., et al. 2014, A&A, 561, L1
Borucki, W. J., Koch, D., Basri, G., et al. 2010, Science, 327, 977
Butler, R. P., Wright, J. T., Marcy, G. W., et al. 2006, ApJ, 646, 505
Carter, J. A., Agol, E., Chaplin, W. J., et al. 2012, Science, 337, 556
Carter, J. A. & Winn, J. N. 2009, ApJ, 704, 51
Carter, J. A., Winn, J. N., Holman, M. J., et al. 2011, ApJ, 730, 82
Charbonneau, D., Brown, T. M., Latham, D. W., & Mayor, M. 2000, ApJ, 529, L45
Claret, A. 2000, A&A, 363, 1081
Cochran, W. D., Fabrycky, D. C., Torres, G., et al. 2011, ApJS, 197, 7
Czesla, S., Huber, K. F., Wolter, U., Schröter, S., & Schmitt, J. H. M. M. 2009, A&A, 505, 1277
Eastman, J., Siverd, R., & Gaudi, B. S. 2010, PASP, 122, 935
Fukui, A., Narita, N., Tristram, P. J., et al. 2011, PASJ, 63, 287
Hartman, J. D., Bakos, G. Á., Kipping, D. M., et al. 2011, ApJ, 728, 138
Høg, E., Fabricius, C., Makarov, V. V., et al. 2000, A&A, 355, L27
Holman, M. J., Fabrycky, D. C., Ragozzine, D., et al. 2010, Science, 330, 51
Huber, K. F., Czesla, S., Wolter, U., & Schmitt, J. H. M. M. 2010, A&A, 514, A39
Ioannidis, P., Huber, K. F., & Schmitt, J. H. M. M. 2016, A&A, 585, A72
Jones, E., Oliphant, T., Peterson, P., et al. 2001, SciPy: Open source scientific tools for Python, http://www.scipy.org
Karoff, C., Knudsen, M. F., De Cat, P., et al. 2016, Nature Communications, 7, 11058
Kjeldsen, H. & Frandsen, S. 1992, PASP, 104, 413
Koch, D. G., Borucki, W. J., Basri, G., et al. 2010, ApJ, 713, L79
Lanza, A. F. 2011, in IAU Symposium, Vol. 273, Physics of Sun and Star Spots, ed. D. Prasad Choudhary & K. G. Strassmeier, 89–95
Lissauer, J. J., Fabrycky, D. C., Ford, E. B., et al. 2011, Nature, 470, 53
Lomb, N. R. 1976, Ap&SS, 39, 447
Maciejewski, G., Dimitrov, D., Neuhäuser, R., et al. 2011, MNRAS, 411, 1204
Mallonn, M. & Strassmeier, K. G. 2016, A&A, 590, A100
Mallonn, M., von Essen, C., Weingrill, J., et al. 2015, A&A, 580, A60
Mandel, K. & Agol, E. 2002, ApJ, 580, L171
Mazeh, T., Nachmani, G., Holczer, T., et al. 2013, ApJS, 208, 16
Patil, A., Huard, D., & Fonnesbeck, C. J. 2010, Journal of Statistical Software, 35, 1
Pont, F., Zucker, S., & Queloz, D. 2006, MNRAS, 373, 231
Rabus, M., Alonso, R., Belmonte, J. A., et al. 2009, A&A, 494, 391
Sanchis-Ojeda, R. & Winn, J. N. 2011, ApJ, 743, 61
Sanchis-Ojeda, R., Winn, J. N., Holman, M. J., et al. 2011, ApJ, 733, 127
Scargle, J. D. 1982, ApJ, 263, 835
Southworth, J., Hinse, T. C., Jørgensen, U. G., et al. 2009, MNRAS, 396, 1023

[4] https://github.com/sczesla/PyAstronomy

Stevenson, K. B., Bean, J. L., Seifahrt, A., et al. 2016, ApJ, 817, 141
Strassmeier, K. G., Granzer, T., Weber, M., et al. 2004, Astronomische Nachrichten, 325, 527
von Essen, C., Cellone, S., Mallonn, M., et al. 2017, A&A, 603, A20
von Essen, C., Ofir, A., Dreizler, S., et al. 2018, A&A, 615, A79
von Essen, C., Schröter, S., Agol, E., & Schmitt, J. H. M. M. 2013, A&A, 555, A92
Wakeford, H. R., Sing, D. K., Kataria, T., et al. 2017, Science, 356, 628
Weber, M., Granzer, T., & Strassmeier, K. G. 2012, in Proc. SPIE, Vol. 8451, Software and Cyberinfrastructure for Astronomy II, 84510K
Zechmeister, M. & Kürster, M. 2009, A&A, 496, 577